Extratropical forcing of El Niño–Southern Oscillation asymmetry

Bruce T. Anderson,[1] Jason C. Furtado,[2] Kim M. Cobb,[3] and Emanuele Di Lorenzo[3]

Received 20 June 2013; revised 29 August 2013; accepted 6 September 2013; published 24 September 2013.

[1] Boreal winter near-surface atmospheric circulations over the Hawaiian region are known to influence the state of the tropical Pacific and initiate the development of El Niño–Southern Oscillation (ENSO) events. Here we show that these same preceding near-surface circulations have an additional influence on the longitudinal position of the resultant ENSO-related sea surface temperatures (SSTs) as well, with warm (cold) events systematically shifted to the east (west) of the typical SST anomalies. In influencing this positioning, these atmospheric circulations in turn modify the near- and far-field climate responses to these SSTs such that during warm events, the typical ENSO-related responses east (west) of the dateline are generally enhanced (reduced); conversely, during cold events, the typical ENSO-related responses are generally reduced (enhanced). The fact that the extratropical atmospheric circulations in question influence the asymmetry of ENSO extremes with a 12 month lead time carries important implications for predicting the socioeconomic impacts of these events. **Citation:** Anderson, B. T., J. C. Furtado, K. M. Cobb, and E. Di Lorenzo (2013), Extratropical forcing of El Niño–Southern Oscillation asymmetry, *Geophys. Res. Lett.*, *40*, 4916–4921, doi:10.1002/grl.50951.

1. Introduction

[2] Changes in sea surface temperatures (SSTs) over the equatorial Pacific associated with the El Niño–Southern Oscillation (ENSO) result in profound shifts in global and regional climates [*Ropelewski and Halpert*, 1986; *Schneider and Steig*, 2008; *Ely et al*., 1993] that impose societal and ecological costs [*Hsiang et al*., 2011; *Stenseth et al*., 2002; *Behrenfeld et al*., 2006]. However, warm (El Niño) and cold (La Niña) events differ in their amplitudes, time evolution, and climatic impacts [*Burgers and Stephenson*, 1999; *Hoerling et al*., 2001; *Larkin and Harrison*, 2002; *Okumura and Deser*, 2010]. In particular, El Niño events are on average larger, less frequent, and shifted to the east relative to La Niña events [*Larkin and Harrison*, 2002]. While numerous studies have put forward mechanisms to explain various aspects of ENSO asymmetry [e.g., *An*, 2009], differences in the east-west position of maximum warming versus cooling, which modulate the mean state and variability of the Pacific [*Sun and Yu*, 2009; *Yu and Kim*, 2011], have not been fully determined [e.g., *Sun and Yu*, 2009].

[3] In this study, we use both observational reanalysis and 1000 years of a coupled climate model run to illustrate the importance of boreal winter sea level pressure (SLP) variations over the Hawaiian region—linked to the North Pacific Oscillation (NPO) [*Walker and Bliss*, 1932; *Rogers*, 1981; *Linkin and Nigam*, 2008]—in explaining these asymmetries in ENSO events. As these SLP variations have also been tied to ENSO event initiation [*Trenberth and Shea*, 1987; *Barnett et al*., 1988; *Vimont et al*., 2001; *Anderson*, 2003], our work enhances the predictability of ENSO events and their associated large-scale climate impacts during the following winter.

2. Data and Methods

[4] Observed oceanic data (i.e., SST and subsurface temperatures) are acquired from the Simple Ocean Data Assimilation (SODA) version 2.2.6 [*Carton and Giese*, 2008] for the period 1872–2008. Observed atmospheric fields (i.e., SLP and near-surface winds) are taken from the twentieth Century Reanalysis V2 (20CRv2) [*Compo et al*., 2011]. To extend the analysis and demonstrate robustness in our findings, we also conduct analyses with a 1000 year preindustrial control run (i.e., greenhouse gas forcing is set to preindustrial levels) of the Community Climate System Model version 4 (CCSM4) (model specifications can be found in *Gent et al*. [2011]) used as part of the Coupled Model Intercomparison Project Phase 5 (CMIP5) [*Taylor et al*., 2012]. The CCSM4 was chosen primarily for two reasons: (1) availability of a very long integration (1000 years), which allows for more statistical significance in results and (2) the model has demonstrable improvement in ENSO variability and teleconnections over its predecessor (CCSM3) and well simulates the SLP precursor pattern to ENSO events of interest in our study [*Deser et al*., 2012].

[5] To quantify the structural difference between ENSO-related SST anomalies, the longitudinal position for all boreal winter (November–January) warm and cold events is determined using the Center of Heat Index (CHI) [*Giese and Ray*, 2011]. The CHI longitude gives the temperature-weighted center of warm (cold) water anomalies ($>0.5°C$ and $< -0.5°C$, respectively) that span at least 50° longitude within the equatorial Pacific, defined as 5°S–5°N and 120°E–70°W; for years in which no such expanse of warm (cold) water is found, the index is undefined. The east-west shift in observed El Niño versus La Niña events, as represented by the CHI, can be seen in Figure 1a. When calculating the CHI within the CCSM4, the temperature threshold value is increased to $(+/-0.5°C)/0.8$ to account for the known amplitude bias in the year-to-year variance of equatorial Pacific SST anomalies compared with observed values from 1900 to 2010 [*Deser et al*., 2012]. Given the structural changes

Additional supporting information may be found in the online version of this article.

[1]Department of Earth and Environment, Boston University, Boston, Massachusetts, USA.
[2]Atmospheric and Environmental Research, Lexington, Massachusetts, USA.
[3]School of Earth and Atmospheric Science, Georgia Institute of Technology, Atlanta, Georgia, USA.

Corresponding author: B. T. Anderson, Department of Earth and Environment, Boston University, Boston, MA 02215, USA. (brucea@bu.edu)

0094-8276/13/10.1002/grl.50951

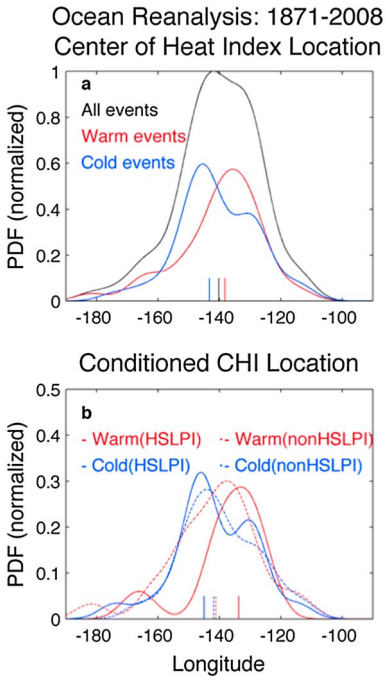

Figure 1. (a) Distribution of the observationally constrained Center of Heat Index (CHI) longitude for warm (red), cold (blue), and all (black) events found in the equatorial Pacific during each November–January from 1872 to 2008. The distributions are determined using a kernel-smoothing density estimate based upon a normal kernel and bin width of 5° longitude. The distribution values for all events (black) are normalized by the maximum value, while those for the warm (red) and cold (blue) events are normalized such that they sum to the black line. Thin, vertical lines on the x axis represent the median longitude of each distribution. (b) Distribution of the CHI longitude for HSLPI-related warm events (HSLPI $< -0.5\sigma$ the previous year; red solid) and HSLPI-related cold events (HSLPI $> 0.5\sigma$ the previous year; blue solid). Red (blue) dashed curves denote non-HSLPI-related warm (cold) ENSO events (see text for details). HSLPI region shown in Figure S1a. Distributions are normalized such that they sum to the total number of warm and cold events, respectively, as found in Figure 1a. Note the change in the y axis scale. Thin, vertical lines on the x axis as in Figure 1a.

between individual ENSO events, we will also calculate a Symmetric ENSO Index and an Asymmetric ENSO Index (SEI and AEI, respectively). The positive (negative) boreal winter CHI events are used to first generate a composite map of warm (cold) event SSTs. Following the lead of *Larkin and Harrison* [2002], we invert the composite anomalies associated with the cold events (here and throughout the paper) by multiplying by −1. The average of the warm and inverted cold composites produces the "Symmetric" anomaly pattern; the difference of the two composites produces the "Asymmetric" anomaly pattern. Selecting the SST anomalies within the equatorial Pacific (120°E–70°W, 5°S–5°N) from the symmetric and asymmetric anomaly patterns, we perform a multivariate spatial regression against each year's November–January anomalies (within the equatorial Pacific). The SEI and AEI values for a particular year are given by the weight of the symmetric and asymmetric patterns that optimally (in a least squares sense) reproduce the actual anomalies for that year.

3. Observational Analysis

[6] To start, we use oceanic and atmospheric reanalysis data to investigate the role of extratropical SLP anomalies in shaping the degree of east-west asymmetry in ENSO extremes. Specifically, we define a SLP index over the Hawaiian region (hereafter the HSLPI) as the area-averaged normalized (by the interannual standard deviation) November–March seasonal-mean SLP anomalies in the region 175°W–140°W, 10°N–25°N [*Anderson*, 2003] (see also Figure S1a in supporting information). We then sort the instrumental record of El Niño extremes into those that are preceded 12 months earlier by low HSLPI ($<-0.5\sigma$) conditions —termed the HSLPI-related warm events—and those that are not—termed the non-HSLPI-related warm events; a similar sorting using high values of HSLPI ($>0.5\sigma$) as a threshold is used to classify La Niña extremes. This analysis reveals marked HSLPI-related asymmetries in the longitudinal positions of the subsequent El Niño and La Niña events such that the mean CHI for HSLPI-related warm events is shifted 11° east with respect to HSLPI-related cold events (Figure 1b) whereas the longitudinal asymmetry is significantly reduced for the non-HSLPI-related extremes (to less than 1°). Applying a two-tailed Kolmogorov-Smirnov goodness-of-fit test reveals that the distributions of the HSLPI-related warm and cold events are significantly different from one another ($p < 0.05$), while the distributions of non-HSLPI-related events cannot be statistically differentiated.

[7] Composite maps of the ocean-atmosphere evolution for HSLPI-related warm and cold events illustrate the relationship between HSLPI anomalies in boreal winter and the asymmetry of ENSO extremes the following winter (Figure 2). In particular, the longitudinal CHI shift described in Figure 1b is readily apparent in the concurrent subsurface heat content anomalies (T(0–300m); Figures 2b and 2e)—a significant precursor to mature ENSO events [*Wyrtki*, 1985; *Jin*, 1997; *Meinen and McPhaden*, 2000; *Newman et al.*, 2011]—even more so than in the subsequent SST anomalies during the mature phase of El Niño and La Niña events themselves.

4. Coupled Climate Model Analysis

[8] The above results suggest that antecedent extratropical SLP anomalies within the southern lobe of the NPO have a significant impact on the asymmetry between mature warm and cold events, with a 1 year lead time. However, the limited length of the observational record constrains our analysis to relatively few events: 29 HSLPI-related warm and cold ENSO extremes, and 50 non-HSLPI-related warm and cold ENSO extremes. Therefore, we analyze the long CCSM4 run to acquire more samples of ENSO events and thus further investigate the statistical robustness of the observed relationship between extratropical North Pacific atmospheric variability and ENSO asymmetry. As in observations, there is an eastward shift (~7°) in the median longitude of the CHI

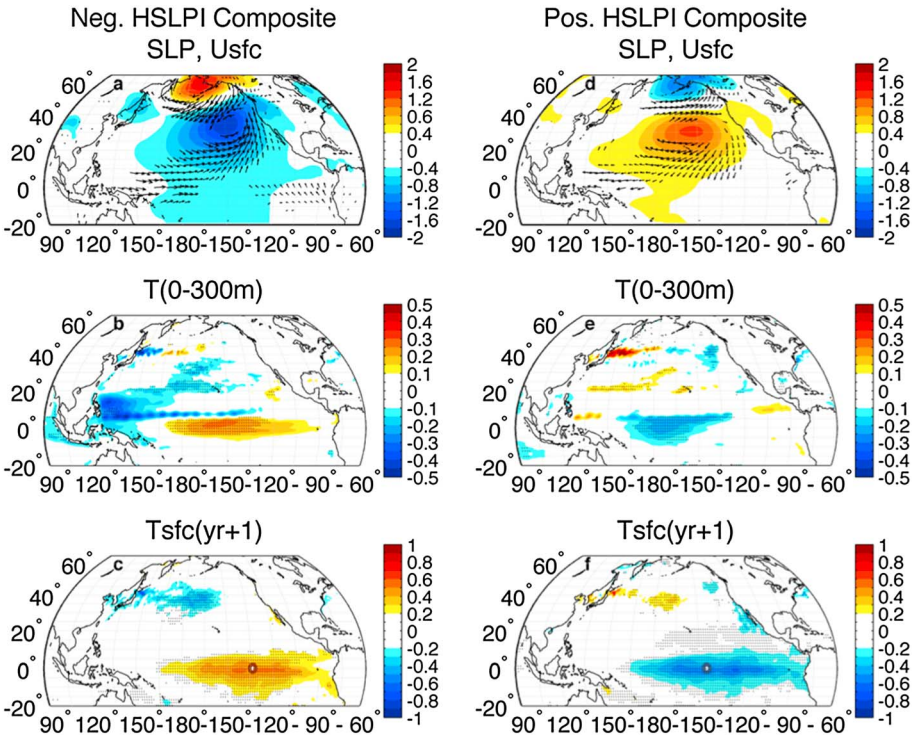

Figure 2. (a) Shading: Mean November–March SLP anomalies from 20CRv2 during years in which HSLPI $< -0.5\sigma$. Minimum contour is +/−0.4hPa; contour interval is 0.2hPa. Vectors: Mean November–March 10m wind vector anomalies from 20CRv2 during years in which HSLPI $< -0.5\sigma$. Only shown are those with an anomalous magnitude that is significant at the 90% confidence limit, based upon a one-sample *t* test of the mean assuming a normal distribution with unknown variance. (b) Shading: Mean November–March subsurface temperature anomalies from SODA, averaged between 0 and 300m, during years in which HSLPI $< -0.5\sigma$. Shading interval is 0.05°C; minimum shading is +/−0.1°C. Stippling indicates regions where composite anomalies are significant at the 90% confidence limit, based upon a one-sample *t* test of the mean assuming a normal distribution with unknown variance. (c) Composite of November–January SST anomalies from SODA when HSLPI $< -0.5\sigma$ the previous year. Shading interval is 0.1°C; minimum shading is +/−0.2°C. Stippling as in Figure 2b. Circle indicates median CHI longitude for all subsequent HSLPI-related warm events, as found in Figure 1b. (d, e, f) Same as Figures 2a, 2b, and 2c except for years in which HSLPI $> 0.5\sigma$. Circle indicates median CHI longitude for all subsequent HSLPI-related cold events.

for HSLPI-related warm events compared with HSLPI-related cold events (Figure 3a). Non-HSLPI-related warm and cold events, however, exhibit a very small longitudinal shift in the CHI (less than 1°; Figure 3b). As before, the distributions of the HSLPI-related warm and cold events are significantly different from one another ($p < 0.001$); further, the distributions of HSLPI-related warm (cold) events and non-HSLPI-related warm (cold) events are also significantly different from each other ($p < 0.025$), indicating the importance of the HSLPI as a precursor for the ENSO SST spatial structure in the model.

[9] The cumulative effect of more eastward HSLPI-related El Niño events and westward HSLPI-related La Niña events results in relatively warm anomalies in the eastern equatorial and off-equatorial Pacific and cool anomalies in the western equatorial/off-equatorial Pacific (Figure 3c). Conversely, SST anomalies associated with the more symmetric, non-HSLPI-related ENSO extremes mostly cancel each other out (Figure 3d). To illustrate more clearly the role of HSLPI anomalies in driving this ENSO-related SST asymmetry, we investigate the relationship between low-frequency variations in ENSO asymmetry and the strength of HSLPI/ENSO coupling in the model simulation (Figure 3e). In general, periods of strong (weak) HSLPI/ENSO coupling coincide with more asymmetry (symmetry) between warm and cold ENSO events. Hence, our model analyses strongly support the HSLPI precursor as a dominant control on mature ENSO event asymmetry with a 1 year lead time.

[10] The significant asymmetry in SST anomalies during HSLPI-related ENSO extremes directly impacts extratropical temperature and precipitation anomalies associated with ENSO (Figure 4). Besides near-surface temperature changes over the equatorial Pacific noted earlier, ENSO asymmetry during HSLPI-related events yields asymmetric cooling over the southern United States and warming over northern North America (Figure 4a) that tends to enhance (by nearly 50%) the linear (or symmetric) response during warm events (Figure S2c). By contrast, over central Eurasia, asymmetric warm anomalies (Figure 4a) negate the cool anomalies associated with the linear response to warm ENSO events (Figure S2c), which is actually extended eastward over northeast Eurasia and the extratropical North Pacific during HSLPI-related warm events (Figure 4a). Enhanced warming also exists over northern South America and India/Southeast Asia during HSLPI-related warm events (cf. Figures 4a and S2c). These asymmetric responses are present even

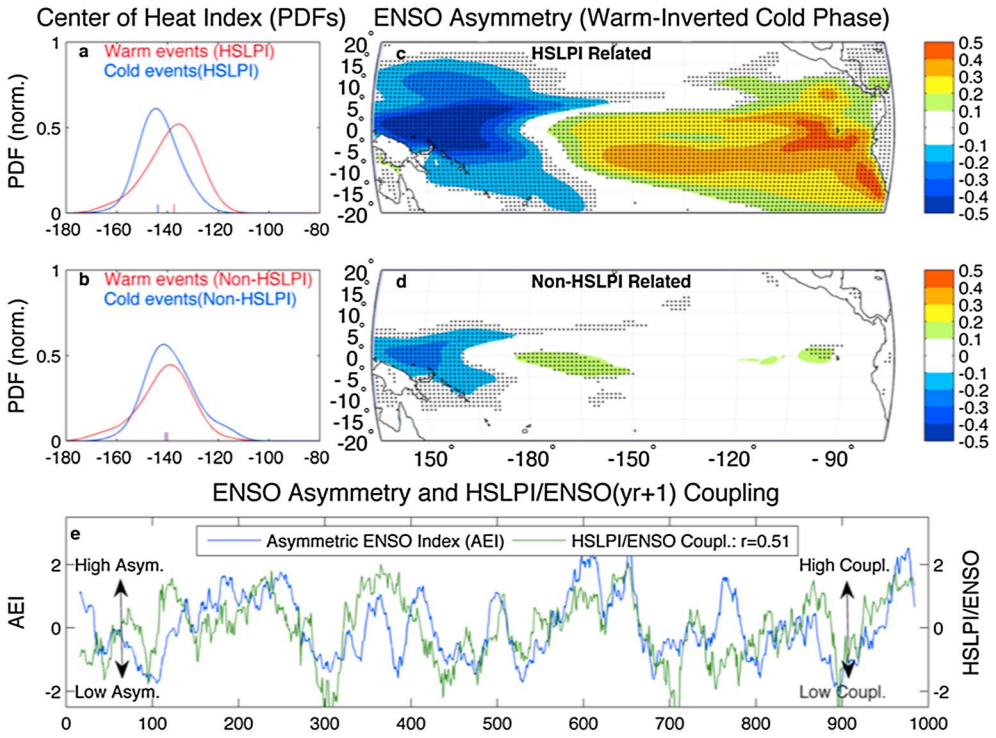

Figure 3. (a) Distribution of the CHI longitude for HSLPI-related warm events (HSLPI $< -0.5\sigma$ the previous year; red solid) and HSLPI-related cold events (HSLPI $> 0.5\sigma$ the previous year; blue solid) from the CCSM4 preindustrial control run. HSLPI region for CCSM4 shown in Figure S1b. The distributions are determined using a kernel-smoothing density estimate based upon a normal kernel and bin width of 5° longitude. Distributions are normalized such that the maximum value for the total number of warm and cold events is set to "1". Thin, vertical lines on the x axis represent the median longitude of each distribution. (b) Same as Figure 3a except for non-HSLPI-related warm (cold) ENSO events. (c) Shading: Difference between the mean November–January surface temperatures anomalies from the CCSM4 for all HSLPI-related warm (174) events and the inverted mean (mean multiplied by -1) for all HSLPI-related cold (163) events, representing the asymmetric difference pattern between HSLPI-related warm and inverted cold event composites. Shading interval is 0.1°C; minimum shading is +/−0.1°C. Stippling indicates regions where composite anomalies are significantly different from one another at the 90% confidence limit, based upon a two-sample t test of the means assuming a normal distribution with unknown variance. (d) Same as Figure 3c except for the difference between the mean November–January surface temperatures anomalies for non-HSLPI-related warm (117) and inverted cold (142) events. (e) Blue line: 30 year running mean value of the standardized anomalies of the November–January Asymmetric ENSO Index (AEI—see text for details). Green line: Time variations in strength of the coupling between the HSLPI and the state of the ENSO 1 year later, as represented by the 30 year running correlations between the November–March HSLPI and the following year's November–January Symmetric ENSO Index (SEI—see text for details). For presentation, the correlation values are multiplied by -1 and standardized. Original values of both time series are shown in Figure S7. The correlation between the AEI and the HSLPI-ENSO coupling index is also shown ($r = 0.51$; $p < 0.05$).

when accounting for possible differences in warm and cold event intensities within the two sets of composites (Figure S3a). In contrast, the asymmetric anomalies associated with non-HSLPI-related events are substantially weaker and less significant than HSLPI-related events (Figures 4c and S3c).

[11] Corresponding composites for precipitation also show substantial asymmetry in anomalous wet and dry conditions during HSLPI-related ENSO extremes (Figure 4b). The eastward shift of the CHI longitude during HSLPI-related warm events influences precipitation across the tropical Indo-Pacific basin (Figure 4b), enhancing the expected warm event wetting in the central and eastern tropical Pacific but offsetting drying in southern India and parts of Southeast Asia, again by up to 50% (Figure S4c). Asymmetric ENSO behavior also projects strongly on the northeastward displacement of the South Pacific Convergence Zone (Figure 4b) and enhances expected dryness across the Amazon during warm events (Figure S4c). Outside the tropical Indo-Pacific, asymmetric ENSO behavior during HSLPI-related warm events enhances wet conditions along the western and eastern North American coasts and parts of central Eurasia (cf. Figures 4b and S4c). For non-HSLPI-related ENSO events (Figure 4d), the asymmetric signatures are substantially reduced in magnitude and less prevalent relative to the HSLPI-related events (Figure 4b). The global precipitation and temperature responses to ENSO asymmetry discussed here can be interpreted in the context of significant differences in the structure of the global atmospheric circulation (supporting information and Figures S5 and S6).

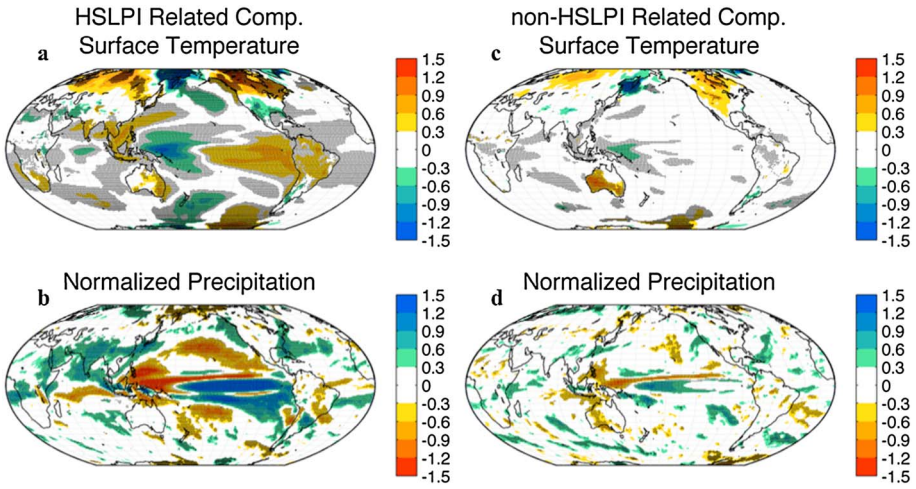

Figure 4. (a) Shading: Difference between the mean November–March near-surface temperature anomalies from the CCSM4 for all November–January HSLPI-related warm (174) events and the inverted mean (mean multiplied by −1) for all HSLPI-related cold (163) events, representing the asymmetric difference pattern between HSLPI-related warm and inverted cold event composites. Individual composite anomalies can be found in Figures S2a and S2b. For clarity, anomalies are multiplied by 2 for comparison with symmetric mean patterns (Figure S2c). Shading interval is 0.3°C; minimum shading is +/−0.3°C. Stippling indicates regions where composite anomalies are significantly different from one another at the 90% confidence limit, based upon a two-sample *t* test of the means assuming a normal distribution with unknown variance. (b) Same as Figure 4a except for normalized precipitation anomalies in which the precipitation anomaly at a given grid point is divided by its year-to-year standard deviation value. Individual composite anomalies and symmetric mean patterns can be found in Figure S4. Shading interval is 0.3σ; minimum shading is +/−0.3σ. (c, d) Same as Figures 4a and 4b except for all November–January non-HSLPI-related warm events (117) and inverted cold events (142).

5. Summary and Discussion

[12] Here we present evidence that North Pacific atmospheric circulations during boreal winter can influence the asymmetric nature of ENSO events 12 months later. Observationally constrained ocean data indicate that El Niño/La Niña events that are preceded by substantial negative/positive SLP anomalies near Hawaii tend to be shifted by 10° in longitude from one another. Conversely, the longitudinal positions of El Niño/La Niña events with no extratropical SLP precursor are nearly identical. The observed relationship between extratropical boreal winter SLP anomalies and ENSO asymmetry is confirmed in a 1000 year preindustrial control simulation of the CCSM4. Further, analyses reveal that a high degree of asymmetry in the spatial footprint of ENSO extremes translates into appreciable differences in ENSO teleconnections with temperature and precipitation effects in many regions of the globe.

[13] Overall, the results of our study indicate that the HSLPI is not only a precursor to ENSO extremes but also contributes fundamentally to the longitudinal structure of the resulting warm and cool events. This asymmetric response of the ENSO system to the SLP precursor serves as an additional test of numerical Earth system models' veracity in representing tropical/extratropical interactions, as well as their potential changes under future global warming. Moreover, as the degree of ENSO asymmetry alters regional climate responses to ENSO extremes and the SLP precursor for this asymmetry appears nearly 1 year earlier, our findings carry important implications for predictability of, and preparedness for, boreal winter climate impacts across North America and Eurasia and monsoonal impacts in Southeast Asia and Australia. Further, the time-varying influence of the HSLPI upon ENSO has important extrapolations to the reconstruction of ENSO activity back in time, which is based upon proxy-derived temperature and precipitation estimates that fall within the spatial footprint of HSLPI-induced regional climate asymmetries identified here. Finally, longitudinal shifts correspond to an increase in event magnitude [e.g., *Sun and Yu*, 2009; *Dommenget et al*., 2013]; accordingly, the median CCSM4 CHI longitudes for the largest warm and cold events (those with absolute magnitudes >1.5°C or approximately the upper quartile) are shifted by ~15° with respect to one another. That these very large events (in the CCSM4) are 3 times more likely to be HSLPI-related than non-HSLPI-related (110 and 37, respectively) suggests HSLPI activity (both during a particular year as well as during periods of extended coupling) may additionally modulate ENSO event intensity, either directly or by shifting the events' longitudinal structures.

[14] **Acknowledgments.** We extend our thanks to Zhengyu Liu and one anonymous reviewer for their constructive and insightful comments. This work was supported by the Department of Energy (DE-SC0004975 to B.T.A.). We acknowledge the World Climate Research Programme's Working Group on Coupled Modelling, which is responsible for CMIP, and we thank the climate modeling groups (listed in Table S1) for producing and making available their model output. For CMIP, the U.S. Department of Energy's Program for Climate Model Diagnosis and Intercomparison provides coordinating support and led development of software infrastructure in partnership with the Global Organization for Earth System Science Portals. Twentieth Century Reanalysis V2 data provided by the NOAA/OAR/ESRL PSD, Boulder, Colorado, USA, from their Web site at http://www.esrl.noaa.gov/psd/. Support for the Twentieth Century Reanalysis Project data set is provided by the U.S. Department of Energy, Office of Science Innovative and Novel Computational Impact on Theory and Experiment (DOE INCITE) program, and Office of Biological and Environmental Research (BER), and by the National Oceanic and Atmospheric Administration Climate Program Office.

[15] The Editor thanks Zhengyu Liu and an anonymous reviewer for assistance evaluating this manuscript.

References

An, S.-I. (2009), A review of interdecadal changes in the nonlinearity of the El Nino-Southern Oscillation, *Theor. Appl. Climatol.*, *97*, 29–40.

Anderson, B. T. (2003), Tropical Pacific sea-surface temperatures and preceding sea level pressure anomalies in the subtropical North Pacific, *J. Geophys. Res.*, *108*(D23), 4732, doi:10.1029/2003JD003805.

Barnett, T., et al. (1988), On the prediction of the El Niño of 1986–1987, *Science*, *241*, 192–196.

Behrenfeld, M. J., et al. (2006), Climate-driven trends in contemporary ocean productivity, *Nature*, *444*, 752–755.

Burgers, G., and D. B. Stephenson (1999), The "normality" of El Nino, *Geophys. Res. Lett.*, *26*, 1027–1030.

Carton, J. A., and B. S. Giese (2008), A reanalysis of ocean climate using Simple Ocean Data Assimilation (SODA), *Mon. Weather Rev.*, *136*, 2999–3017.

Compo, G. P., et al. (2011), The Twentieth Century Reanalysis Project, *Q. J. R. Meteorol. Soc.*, *137*, 1–28.

Deser, C., et al. (2012), ENSO and Pacific decadal variability in the Community Climate System Model Version 4, *J. Clim.*, *25*, 2622–2651.

Dommenget, D., T. Bayr, and C. Frauen (2013), Analysis of the non-linearity in the pattern and time evolution of El Niño Southern Oscillation, *Clim. Dyn.*, *40*, 2825–2847.

Ely, L. L., et al. (1993), A 5000-year record of extreme floods and climate-change in the Southwestern United States, *Science*, *262*, 410–412.

Gent, P. R., et al. (2011), The Community Climate System Model Version 4, *J. Clim.*, *24*, 4973–4991.

Giese, B. S., and Ray, S. (2011), El Niño variability in simple ocean data assimilation (SODA), 1871–2008, *J. Geophys. Res.*, *116*, C02024, doi:10.1029/2010JC006695.

Hoerling, M. P., A. Kumar, and T. Y. Xu (2001), Robustness of the nonlinear climate response to ENSO's extreme phases, *J. Clim.*, *14*, 1277–1293.

Hsiang, S. M., K. C. Meng, and M. A. Cane (2011), Civil conflicts are associated with global climate, *Nature*, *476*, 438–441.

Jin, F.-F. (1997), An equatorial ocean recharge paradigm for ENSO. 1. Conceptual model, *J. Atmos. Sci.*, *54*, 811–829.

Larkin, N. K., and D. E. Harrison (2002), ENSO warm (El Niño) and cold (La Niña) event life cycles: Ocean surface anomaly patterns, their symmetries, asymmetries, and implications, *J. Clim.*, *15*, 1118–1140.

Linkin, M. E., and S. Nigam (2008), The North Pacific Oscillation–West Pacific teleconnection pattern: Mature-phase structure and winter impacts, *J. Clim.*, *21*, 1979–1997.

Meinen, C. S., and M. J. McPhaden (2000), Observations of warm water volume changes in the equatorial Pacific and their relationship to El Niño and La Niña, *J. Clim.*, *13*, 3551–3559.

Newman, M., M. A. Alexander, and J. D. Scott (2011), An empirical model of tropical ocean dynamics, *Clim. Dyn.*, *37*, 1823–1841.

Okumura, Y. M., and C. Deser (2010), Asymmetry in the duration of El Niño and La Niña, *J. Clim.*, *23*, 5826–5843.

Rogers, J. C. (1981), The North Pacific Oscillation, *J. Climatol.*, *1*, 39–57.

Ropelewski, C. F., and M. S. Halpert (1986), North American precipitation and temperature patterns associated with the El Niño/Southern Oscillation (ENSO), *Mon. Weather Rev.*, *114*, 2352–2362.

Schneider, D. P., and E. J. Steig (2008), Ice cores record significant 1940s Antarctic warmth related to tropical climate variability, *Proc. Natl. Acad. Sci. U. S. A.*, *105*, 12,154–12,158.

Stenseth, N. C., et al. (2002), Ecological effect of climate fluctuation, *Science*, *297*, 1292–1296.

Sun, F., and J.-Y. Yu (2009), A 10–15-yr modulation cycle of ENSO intensity, *J. Clim.*, *22*, 1718–1735.

Taylor, K. E., R. J. Stouffer, and G. A. Meehl (2012), An overview of CMIP5 and the experiment design, *Bull. Am. Meteorol. Soc.*, *93*, 485–498.

Trenberth, K. E., and D. J. Shea (1987), On the evolution of the Southern Oscillation, *Mon. Weather Rev.*, *115*, 3078–3096.

Vimont, D. J., S. Battisti, and A. C. Hirst (2001), Footprinting: A seasonal connection between the tropics and mid-latitudes, *Geophys. Res. Lett.*, *28*, 3923–3926.

Walker, G. T., and E. W. Bliss (1932), World Weather V, *Mem. Roy. Meteor. Soc.*, *4*, 53–83.

Wyrtki, K. (1985), Water displacements in the Pacific and the genesis of El Niño cycles, *J. Geophys. Res.*, *90*, 7129–7132.

Yu, J.-I., and S. T. Kim (2011), Reversed spatial asymmetries between El Niño and La Niña and their linkage to decadal ENSO modulation in CMIP3 models, *J. Clim.*, *24*, 5423–5434.